ChemComm

Efficient photoluminescence of isotropic rare-earth oxychloride nanocrystals from a solvothermal route

Journal:	*ChemComm*
Manuscript ID	CC-COM-01-2020-000113.R1
Article Type:	Communication

COMMUNICATION

Efficient photoluminescence of isotropic rare-earth oxychloride nanocrystals from a solvothermal route

Received 00th January 20xx,
Accepted 00th January 20xx

DOI: 10.1039/x0xx00000x

Guillaume Gouget,[a] Morgane Pellerin,[b] Lauriane Pautrot-D'Alençon,[b] Thierry Le Mercier,[b] and Christopher B. Murray*[a]

Eu^{3+}-doped sub-10 nm LaOCl nanocrystals with 43 % photoluminescence quantum yield were prepared by solvothermal synthesis from hydrated rare-earth chlorides. As-obtained nanocrystals are nearly spherical, monodisperse and stable as colloidal dispersions. These combined features should intensify the interest for nanocrystalline rare-earth oxyhalides and their optical properties.

For several decades, rare-earth (RE) oxyhalides (REOX) have been investigated for a variety of applications including bio-imaging,[1] small molecule sensing,[2] high-energy photon detection,[3,4] heterogeneous catalysis in the gas or liquid phase,[5–9] halide ion conduction,[10] and light-emitting displays.[11] REOXs are attractive for their luminescence properties: (i) several REs can be readily combined in a single REOX structure with various proportions, yielding optimized luminescence features,[1,4,12-16] and (ii) REOXs are low phonon energy hosts (e.g. ca. 440 cm^{-1} for LaOCl),[6,17] which prevents the excited RE-emitting centers from luminescence quenching *via* multi-phonon relaxation. PL excitation may occur in various energies ranges, from infrared (IR) all the way to X-rays. LaOCl bandgap is 4.17 eV according to density functional theory (DFT) calculation,[18] and it displays several absorption features in the UV range.[19,20] IR and visible light directly excite REs emitters, whereas UV or X-Ray light excitation occur via the absorption from LaOCl followed by energy transfer to the RE emitter. LaOCl then sensitizes RE emission in the UV or X-Ray range.

The production of stable colloidal dispersions of REOX nanocrystals (NCs) in the sub-20 nm regime is beneficial for their processability (e.g. formation of thin close-packed films) and for bio-compatibility.[21] The search for routes to REOX NCs has become more intense in the past ten years. They were recently reviewed by Sarbajit Banerjee and co-workers.[22] The LaOCl NCs systematically display platelet morphologies, in relation with their tetragonal structure (*c* axis orthogonal to the most expressed facets). LaOCl structure (space group P4/nmm, No. 129, Fig. 1) comprises layers of Cl anions intercalated between slabs of LaO units (formally +1 charge·$unit^{-1}$) along the *ab* plane. Each La atom is coordinated to 4 O and 5 Cl in a C_{4v} symmetry environment. The separation of cation sites along *c* limits cross-relaxation mechanisms between emitting RE^{3+} centers.[4,13,23] The lamellar structure is also attractive for Cl ion conduction.[10] Structural anisotropy is thus beneficial for optical and transport properties. In 2009, Du et al. reported ultra-thin Eu^{3+}-doped LaOCl nanoplates (aspect ratio from 3.2 to 4.4). Hydrated RE trichloroacetates single-source precursors were decomposed in the presence of various amines.[24] The relatively low PL quantum yield (PLQY) of 5 % Eu^{3+}-doped LaOCl nanoplates (PLQY = 2.8 %) was attributed to the predominant non-radiative pathways due to high-frequency vibrations of long-chain amine ligands on the surface of the nanoplates. Anisotropic morphologies can have negative consequences on the photoluminescence (PL). More isotropic (ideally cubic or spherical) morphologies would provide a lower surface-to-volume ratio, i.e. a higher volume for Eu^{3+} centers to be spatially separated from the interface, and consequently higher PL efficiency.

Herein we report a synthetic route towards sub-10 nm spherical LaOCl colloidal NCs, relying on the reaction of hydrated chloride salts and oleylamine (OLA) at 220 °C. Monodisperse samples were obtained, leading to self-assembling of the dispersed crystals into close-packed films.

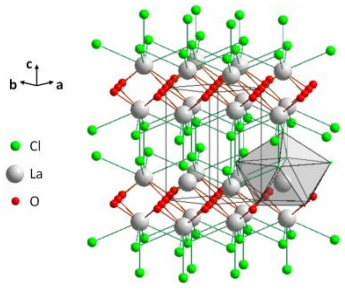

Fig. 1 Structure of LaOCl (P4/nmm, No. 129). The grey polyhedron highlights La 9-fold coordinated environnement.

[a] *Department of Chemistry, University of Pennsylvania, Philadelphia, Pennsylvania 19104, United States.*
[b] *Solvay, Research and Innovation Center Paris, F-93308, Aubervilliers, France.*
[c] *Address here.*
Electronic Supplementary Information (ESI) available: experimental section and additional data, Fig. S1-S9. See DOI: 10.1039/x0xx00000x

Using Eu^{3+}-doped (5 %) LaOCl NCs as a case study, PL efficiency was improved, as detailed later. The correlations between synthetic conditions, morphology and luminescence properties of the NCs were discussed.

Details of the syntheses are reported in the Experimental Section of Supporting Information. Briefly, hydrated RE chlorides (starting either from $LaCl_3.7H_2O$ only or a mix of $LaCl_3.7H_2O$ and $EuCl_3.6H_2O$ (La:Eu molar ratio of 19:1)) were dissolved in methanol (MeOH) prior to the addition of (OLA) in air, at RT. The MeOH was evaporated and the mixture was then degassed for 1 h at 120°C and 1 Torr. The reaction was held at 220 °C during 1 h under N_2, then oleic acid (OA) was injected to the mixture and the reactant medium was cooled to RT by blowing cool air over the vessel. Purification was performed by two successive (i) additions of toluene and MeOH followed by (ii) centrifugation to yield a precipitate and (iii) removal of the supernatant. The final white pellet was redispersed in chloroform, leading to a clear colorless solution. X-ray diffraction (XRD) patterns in Fig. 2a were performed on films obtained by dropcasting both dispersions on glass slides. In both cases, LaOCl was unambiguously identified as a pure phase (see also Supporting Information, Fig. S1). Significant broadening of the peaks were attributed to small crystalline domains. Using the Scherrer formula, apparent crystal sizes from XRD diagrams were 6.6±0.3 and 7.1±0.6 nm for the Eu^{3+}-doped and undoped samples, respectively.[25] Energy dispersive spectroscopy (EDS) (Fig. S2) indicated a molar ratio RE:Cl = 1.00, in agreement with the expected value for REOCl. Focusing on Eu^{3+}-doped LaOCl, the effective Eu insertion rate (Eu:(La+Eu) molar ratio) was 4.8±0.2 %, according to elemental analysis by inductive coupled plasma-optical emission spectrometry (ICP-OES) measurements. The insertion rate of Eu corresponds to the initial 19:1 (La:Eu) molar ratio.

Transmission electron microscopy (TEM, Fig. 2b and c) showed ordered spherical NCs (see also Fig. S3). Selected area electron diffraction (Fig. 2b, inset) and HRTEM (Fig. S4) confirmed that the NCs have the oxychloride structure, as observed by XRD. Their average size was 8.2±1.1 nm, according to TEM. This value was 24 % higher than the apparent crystal size calculated from XRD. The deviation was attributed to underestimation of apparent crystal size, due to crystals strains contributing to XRD peak broadening. HRTEM (Fig. S4) confirmed that the NCs are monocrystalline. The average aspect ratio was 1.1 according to TEM. The NCs self-assembled upon dropcasting the dispersion on a TEM grid. Monolayers (and bilayers, Fig. S3) with hexagonal packing occured, as observed on the fast Fourier transform (FFT, Fig. 2c, inset). The average center-to-center distance between two neighboring NCs was 10.0 nm, so the shortest edge-to-edge distance was 1.8 nm. This separation length is typically observed for NCs capped with OLA or OA.[26] Fourier transform infra-red spectroscopy indicated that OLA binds to the surface of the NCs after the purification steps (Fig. S5). OA was added at the end of the heating step at 220 °C to avoid irreversible precipitation in the early stages of the purification. It was washed away in the final product, as confirmed by FTIR.

Hydrated lanthanum chloride was used for the first time as a precursor to LaOCl NCs. The synthesis was performed at 220 °C. Alternative routes based on the solvothermal decomposition of RE alkoxides or haloalkoxide intermediates are reported between 300 and 330 °C.[24,30] Other routes require annealing steps above 500 °C.[6,27–29] $LaCl_3.7H_2O$ partially dehydrates between 50 and 200 °C in argon atmosphere,[31] and it yields LaOCl and $LaCl_3$ as competitive products.[32] The precursor contains La-Cl and La-O bonds already formed in the initial precursor, as opposed to previously reported routes.[22] We degassed the mixture of $LaCl_3.7H_2O$ and OLA at 120 °C prior to the reaction at 220 °C. At the end of the degassing step, La probably maintained a Cl- and O-rich first coordination sphere. A lower temperature of synthesis is then explained by a reaction path involving successive dehydrations of the intermediate, instead of the decomposition of an alkoxide. Near-spherical LaOCl NCs (aspect ratio of 1.1) were synthetized, while nanoplates were obtained in previous reports.[22] The anisotropic morphology was related to the layered structure of LaOCl (tetragonal crystal cell) along the *c* axis. Prefered growth along <110> directions was observed when LaOCl ultrathin nanoplates (aspect ratio 4.0) were synthetized from $La(CCl_3COO)_3$ with OLA.[24] In contrast, our study provided an example of isotropic morphology, which we attributed to equal growth rates along the inequivalent directions. We propose that the reactivity of intermediate species dictates the relative growth rates, then resulting in the difference in shapes between previous work[24] and ours. The nature of the intermediate species remains unclear, however $LaCl_3.7H_2O$ probably reacted into a Cl- and O-rich monomer, which was responsible for lower temperatures of synthesis and near-spherical morphologies. Future investigations on intermediate species should be performed to better understand and control shapes of LaOCl NCs. The stability of the NCs was confirmed by XRD and TEM on samples stored 18 months in air (Fig. S6). GdOCl and LaOBr NCs were also synthetized by reacting gadolinium chloride and lanthanum bromide (Fig. S7 and S8, respectively) in OLA.

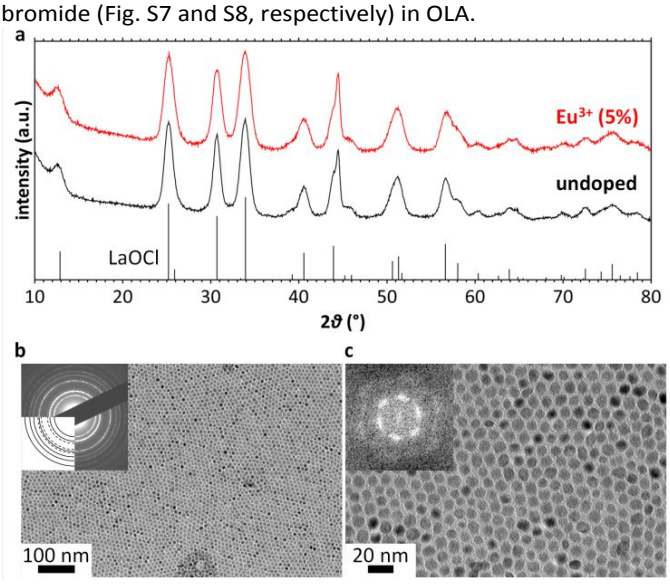

Fig. 2 Structural characterization of LaOCl NCs. a) XRD patterns of undoped and 5 % Eu^{3+}-doped samples. TEM pictures of b) (inset: SAED) and c) (inset: FFT) 5 % Eu^{3+}-doped sample.

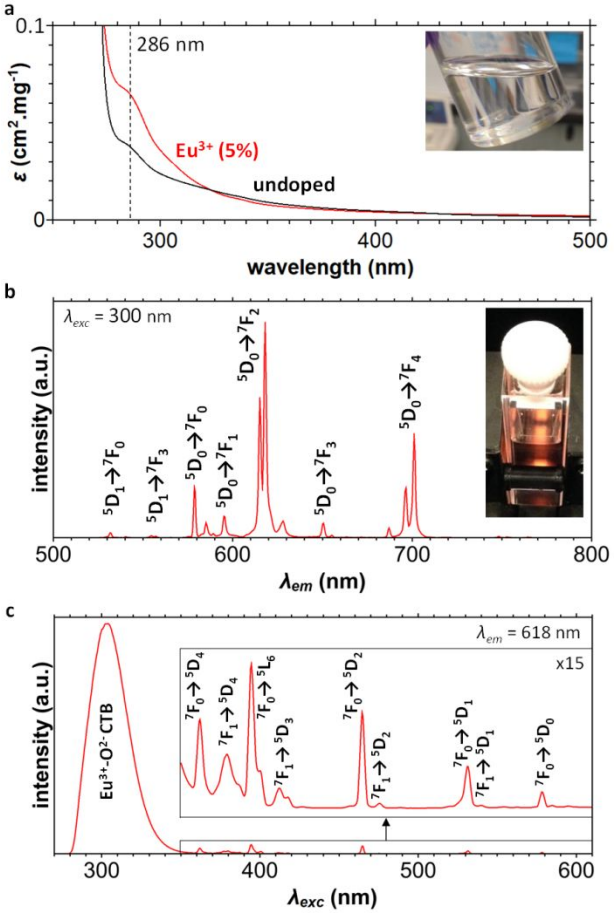

Fig. 3 Optical characterization of LaOCl NCs dispersed in chloroform. a) mass extinction coefficient spectra of undoped and 5 % Eu^{3+}-doped samples, picture of a dispersion in inset. b) PL (inset: dispersion irradiated at 300 nm) and c) PL excitation spectra of 5 % Eu^{3+}-doped sample.

A controlled amount of Eu^{3+} doping was achieved by introducing the desired ratio of RE precursors at the beginning of the synthesis. Mass extinction coefficients of the Eu^{3+}-doped and undoped sample dispersions were compared on Fig. 3a. Neither showed significant light absorption above 400 nm, yielding transparent solutions, as observed in inset. Both doped and undoped samples displayed a peak at 286 nm, before the mass extinction coefficient dramatically increases around 270 nm. These features were attributed to LaOCl, as observed in previous work.[18-20] The slope of absorption front edge was sharper for the undoped sample than for the doped one. An additional broad contribution was detected for the Eu^{3+}-doped sample between 280 and 330 nm. This feature was also observed in other Eu^{3+}-doped LaOCl materials.[18,19] The optical bandgap of undoped LaOCl sample determined by the Tauc method (Fig. S9) was 4.11 eV.[33] The value was close to the one calculated for LaOCl structure from DFT (4.17 eV).[18] The PL spectrum of Eu^{3+}-doped LaOCl spherical NCs excited at λ_{exc} = 300 nm (Fig. 3b) showed narrow emission peaks in the visible region, with a maximized intensity at λ_{em} = 618 nm. It was responsible for the red color of the dispersion under UV irradiation. Each peak was attributed to Eu^{3+} 4f-4f inner transitions (energy diagram in Fig. S10), and labeled accordingly. Focusing on $^5D_0 \rightarrow {}^7F_2$ transition, two main peaks are detected at 615 and 618 nm due to Stark splitting.[34,35] In the case of LaOCl nanoplates,[24] inversion of relative intensity occured in favour of the lower wavelength, which was attributed to a lower symmetry of Eu^{3+} in a distorted environment compared to bulk crystalline sample.[36,37] In contrast, here the LaOCl NCs display luminescence features similar to the bulk phase, suggesting less distortion of Eu^{3+} environment from C_{4v} symmetry (Fig. 1). The PL excitation spectrum was performed at λ_{em} = 618 nm (Fig. 3c). The main broad contribution centered on 300 nm was related to charge-transfer band (CTB) from O 2p to Eu 4f orbitals.[29] The CTB was responsible for the absorption feature between 280 and 330 nm in Eu^{3+}-doped LaOCl (Fig. 3a).[18] The narrower and weaker peaks above 350 nm were due to Eu^{3+} 4f-4f excitations. The emission spectrum at λ_{exc} = 395 nm (corresponding to Eu^{3+} $^7F_0 \rightarrow {}^5L_6$ transition) in Fig. S11 showed a set of emission peaks similar to the peaks observed at λ_{exc} = 300 nm (Fig. 3b).

The efficiency of radiative recombination pathways for Eu^{3+} in LaOCl NCs dispersed in chloroform was probed by PL decay and absolute PLQY measurements (Fig. 4). The PL decay at 618 nm was fit with a single exponential component (χ^2 = 1.07). The lifetime of excited states was 1.0 ms, which was 33 % longer than for Eu^{3+}-doped LaOCl nanoplates (0.75 ms).[24] The lifetime of Eu^{3+} excited states increased, i.e. the rate of non-radiative relaxation decreased. The absolute PLQY was calculated from Equation (1), using an integrating sphere:

$$PLQY_{\lambda_{exc}} = \frac{N_{em}}{N_{abs}} \quad (1),$$

where N_{abs} is the number of photons absorbed by the sample, N_{em} the number of photons emitted and λ_{exc} the wavelength of excitation. These quantities were calculated as the intensity difference between the Eu^{3+}-doped sample and the solvent as reference, for the scattered light (N_{abs}) and the emitted light (N_{em}). Intensities of absorption and emission were plotted as a function of wavelength in Fig. 4b at λ_{exc} = 300 nm, corresponding to the excitation in the O 2p→Eu 4f CTB. The associated $PLQY_{300}$ is 43 %. A similar experiment at λ_{exc} = 395 nm (direct Eu^{3+} $^7F_0 \rightarrow {}^5L_6$ excitation) leads to $PLQY_{395}$ = 14 %. The $PLQY_{395}$ was 5 times higher than reported perviously for LaOCl nanoplates.[24] Higher PL efficiency is observed for near-spherical NCs (aspect ratio of 1.1), as evidenced by lifetime and PLQY measurements. PL quenching is due to non-radiative recombination taking place at the surface of the nanoparticles. The spherical morphology minimizes the surface-to-volume ratio of the NCs. The increase in lifetime and PLQY were then attributed to emissive centers (Eu^{3+}) being, in average, further away from the surface. Colloidal YVO_4:Eu phosphors display a $PLQY_{280}$ up to 38 % after optimization of Eu insertion rate (15 %).[38] The best PL efficiency of YVO_4:Eu is close to LaOCl:Eu without Eu content optimization, which should be addressed in future works.

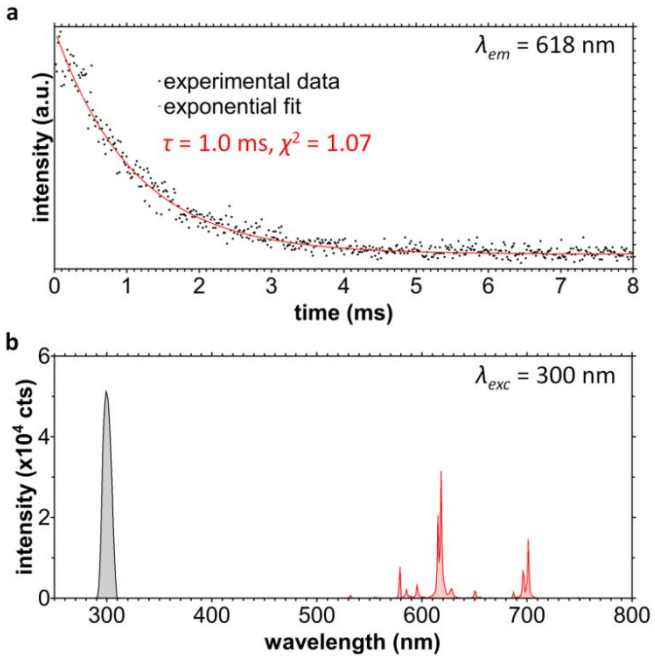

Fig. 4 PL efficiency of Eu^{3+} emission in LaOCl NCs. a) PL decay diagram from excitation at 378 nm, and fitted with a single exponential function. b) light intensity absorbed (black) and emitted (red) by the sample exposed at λ_{exc} = 300 nm in an integrating sphere.

In summary, monodisperse sub-10 nm LaOCl spherical NCs have been obtained for the first time, starting from hydrated RE chlorides and using lower temperatures than previously reported. PL efficiency was improved by accessing isotropic morphologies, as confirmed by longer PL lifetime and higher PLQY. This work stresses the importance of exploring new synthetic methods to diversify morphologies of LaOCl NCs, which yields improved optical properties. In addition to their processability, exemplified by the formation of close-packed NCs films, isotropic LaOCl NCs doped with RE emitters should be highly advantageous in various applications relying on their optical properties. They can be further improved by different strategies: (i) delineating conditions favoring isotropic morphologies for REOX NCs (ii) improving the crystallinity of the nanoparticles, and (iii) forming a protective crystalline shell around the NCs. These strategies all highlight the need of more experimental work on this new route, together with a better understanding of the intermediate species involved during the synthesis.

Conflicts of interest

There are no conflicts to declare.

Notes and references

1 T. Konishi, M. Shimizu, Y. Kameyama and K. Soga, J. Mater. Sci. Mater. Electron., 2007, **18**, 183–186.
2 A. Marsal, G. Dezanneau, A. Cornet and J. R. Morante, Sensors Actuators, B Chem., 2003, **95**, 266–270.
3 J. Rabatin, US patent, 375814, 1972.
4 G. R. Waetzig, G. A. Horrocks, J. W. Jude, G. V. Villalpando, L. Zuin and S. Banerjee, Inorg. Chem., 2018, **57**, 5842–5849.
5 H. Yasuda, L.-N. He and T. Sakakura, J. Catal., 2002, **209**, 547–550.
6 S. G. Podkolzin, E. E. Stangland, M. E. Jones, E. Peringer and J. A. Lercher, J. Am. Chem. Soc., 2007, **129**, 2569–2576.
7 A. W. A. M. van der Heijden, A. J. M. Mens, R. Bogerd and B. M. Weckhuysen, Catal. Letters, 2008, **122**, 238–246.
8 P. Afanasiev, M. Aouine, C. Deranlot and T. Epicier, Chem. Mater., 2010, **22**, 5411–5419.
9 Q. Xie, Y. Wang, B. Pan, H. Wang, W. Su and X. Wang, Catal. Commun., 2012, **27**, 21–25.
10 N. Imanaka, K. Okamoto and G. Adachi, Angew. Chemie Int. Ed., 2002, **41**, 3890–3892.
11 G. Li and J. Lin, Chem. Soc. Rev., 2014, 43, 7099–7131.
12 D. Kim, J. R. Jeong, Y. Jang, J.-S. Bae, I. Chung, R. Liang, D.-K. Seo, S.-J. Kim and J.-C. Park, *Phys. Chem. Chem. Phys.*, 2019, **21**, 1737–1749.
13 G. R. Waetzig, G. A. Horrocks, R. D. Davidson, J. W. Jude, G. V. Villalpando, L. Zuin and S. Banerjee, J. Phys. Chem. C, 2018, **122**, 16412–16423.
14 G. Li, Z. Hou, C. Peng, W. Wang, Z. Cheng, C. Li, H. Lian and J. Lin, Adv. Funct. Mater., 2010, **20**, 3446–3456.
15 J. Hölsä, Chem. Phys. Lett., 1984, 112, 246–248.
16 Z. Xia, J. Li, Y. Luo and L. Liao, J. Am. Ceram. Soc., 2012, **95**, 3229–3234.
17 J. Hölsä, E. Kestilä, K. Koski and H. Rahiala, J. Alloys Compd., 1995, **225**, 193–197.
18 L. Lv, T. Wang, S. Li, Y. Su and X. Wang, CrystEngComm, 2016, **18**, 907–916.
19 D. Kim, S. Park, S. Kim, S.-G. Kang and J.-C. Park, Inorg. Chem., 2014, **53**, 11966–11973.
20 A. A. Dakhel, J. Solid State Chem., 2016, **241**, 219–224.
21 M. A. Boles, D. Ling, T. Hyeon and D. V. Talapin, Nat. Mater., 2016, **15**, 141–153.
22 M. Udayakantha, P. Schofield, G. R. Waetzig and S. Banerjee, J. Solid State Chem., 2019, **270**, 569–592.
23 G. R. Waetzig, G. A. Horrocks, J. W. Jude, L. Zuin and S. Banerjee, Nanoscale, 2016, **8**, 979–986.
24 Y. P. Du, Y. W. Zhang, L. D. Sun and C. H. Yan, J. Am. Chem. Soc., 2009, **131**, 3162–3163.
25 A. L. Patterson, Phys. Rev., 1939, **56**, 978-982.
26 X. Ye, J. Chen, M. Engel, J. A. Millan, W. Li, L. Qi, G. Xing, J. E. Collins, C. R. Kagan, J. Li, S. C. Glotzer and C. B. Murray, Nat. Chem., 2013, **5**, 466–473.
27 E. Peringer, M. Salzinger, M. Hutt, A. A. Lemonidou and J. A. Lercher, Top. Catal., 2009, **52**, 1220–1231.
28 G. Li, C. Li, C. Zhang, Z. Cheng, Z. Quan, C. Peng and J. Lin, J. Mater. Chem., 2009, **19**, 8936.
29 Q. Kong, J. Wang, X. Dong, W. Yu and G. Liu, J. Mater. Sci. Mater. Electron., 2013, **24**, 4745–4756.
30 S. W. Depner, K. R. Kort, C. Jaye, D. A. Fischer and S. Banerjee, J. Phys. Chem. C, 2009, **113**, 14126–14134.
31 D. K. Sahoo, R. Mishra, H. Singh and N. Krishnamurthy, J. Alloys Compd., 2014, **588**, 578–584.
32 J. E. Powell and H. R. Burkholder, J. Inorg. Nucl. Chem., 1960, **14**, 65–70.
33 J. Tauc, R. Grigorovici and A. Vancu, Phys. status solidi, 1966, **15**, 627–637.
34 K. Binnemans, Coord. Chem. Rev., 2015, **295**, 1–45.
35 P. D. Dragic, M. Cavillon and J. Ballato, Appl. Phys. Rev., 2018, **5**, 041301.
36 H. Wang, M. Uehara, H. Nakamura, M. Miyazaki and H. Maeda, Adv. Mater., 2005, **17**, 2506–2509.
37 D. Tu, Y. Liu, H. Zhu, R. Li, L. Liu and X. Chen, Angew. Chemie Int. Ed., 2013, **52**, 1128–1133.
38 A. Huignard, T. Gacoin and J.-P. Boilot, *Chem. Mater.*, 2000, **12**, 1090–1094.

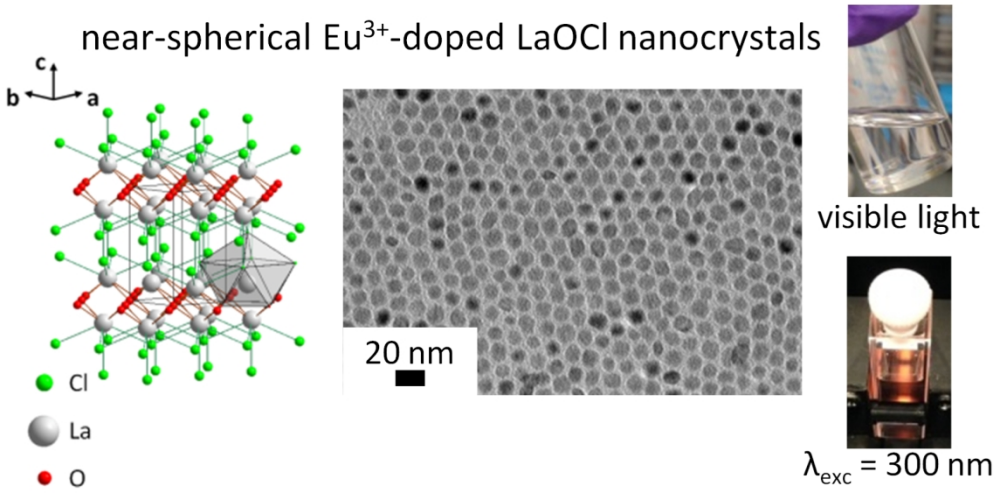
near-spherical Eu^{3+}-doped LaOCl nanocrystals
c
b
a
Cl
La
O
20 nm
visible light
λ_{exc} = 300 nm